



HAL
open science

Atomic force microscopy characterization of polyethylene terephthalate grafting with poly(styrene sulfonate)

Tuan Ngoc Nguyen, Vincent Humblot, Veronique Migonney, Raphaël Lévy

► **To cite this version:**

Tuan Ngoc Nguyen, Vincent Humblot, Veronique Migonney, Raphaël Lévy. Atomic force microscopy characterization of polyethylene terephthalate grafting with poly(styrene sulfonate). *Nanotechnology*, 2022, 10.1088/1361-6528/ac50ef . hal-03560348

HAL Id: hal-03560348

<https://hal.science/hal-03560348v1>

Submitted on 7 Feb 2022

HAL is a multi-disciplinary open access archive for the deposit and dissemination of scientific research documents, whether they are published or not. The documents may come from teaching and research institutions in France or abroad, or from public or private research centers.

L'archive ouverte pluridisciplinaire **HAL**, est destinée au dépôt et à la diffusion de documents scientifiques de niveau recherche, publiés ou non, émanant des établissements d'enseignement et de recherche français ou étrangers, des laboratoires publics ou privés.

1 Atomic force microscopy characterization of polyethylene 2 terephthalate grafting with poly(styrene sulfonate)

3 Tuan Ngoc Nguyen¹; Vincent Humblot²; Véronique Migonney^{1*}; Raphaël Lévy^{3*}

4 ¹Laboratory of Chemistry, Structures, Properties of Biomaterials and Therapeutic Agents
5 (CSPBAT), UMR CNRS 7244, Sorbonne Paris Nord University, France

6 ² Institut FEMTO-ST UMR CNRS 6174, Université Bourgogne Franche-Comté, 15B Avenue des
7 Montboucons, 25030 Besançon, France

8 ³Université Sorbonne Paris Nord and Université de Paris, INSERM, LVTS, F-75018 Paris,
9 France

10 Authors

11 Tuan Ngoc Nguyen: ngoctuan.nguyen@univ-paris13.fr; Vincent Humblot:
12 vincent.humblot@femto-st.fr; Raphaël Lévy: raphael.levy@univ-paris13.fr; Véronique
13 Migonney: veronique.migonney@univ-paris13.fr

14 Corresponding Authors

15 Prof. Raphaël Lévy (raphael.levy@univ-paris13.fr) Université Sorbonne Paris Nord and
16 Université de Paris, INSERM, LVTS, F-75018 Paris, France

17 Prof. Véronique Migonney (veronique.migonney@univ-paris13.fr): Laboratory of Chemistry,
18 Structures, Properties of Biomaterials and Therapeutic Agents, Université Sorbonne Paris
19 Nord, 99 Avenue JB Clément, 93430 Villetaneuse, France

21 Abstract

22 Polyethylene terephthalate (PET) is widely used to elaborate biomaterials and medical
23 devices in particular for long-term implant applications but tuning their surface properties
24 remains challenging. We investigate surface functionalization by grafting poly(sodium 4-
25 styrene sulfonate, PNaSS) with the aim of enhancing protein adhesion and cellular activity.

26 Elucidating the topography and molecular level organization of the modified surfaces is
27 important for understanding and predicting biological activity. In this work, we explore
28 several grafting methods including thermal grafting, thermal grafting in the presence of
29 Mohr's salt, and UV activation. We characterize the different surfaces obtained using atomic
30 force microscopy (AFM), contact angle (CA), and X-ray photoelectron spectroscopy (XPS).
31 We observe an increase in the percentage of sulfur atoms (XPS) that correlates with changes
32 in (CA), and we identify by AFM characteristic features, which we interpret as patches of
33 polymers on the PET surfaces. This work demonstrates tuning of biomaterials surface by
34 functionalization and illustrates the capability of atomic force microscopy to provide insights
35 into the spatial organization of the grafted polymer.

36 **Keywords:** Peakforce Quantitative Nano-mechanical Properties (PF-QNM); Polyelectrolyte
37 brushes; Polyethylene Terephthalate (PET), Poly(sodium 4-styrene sulfonate (PNaSS)

38

39 1. Introduction

40 Polyesters, in particular polyethylene terephthalate (PET), are used extensively in medical
41 devices. Surface functionalization is often required to improve biological properties. Poly
42 (sodium 4-styrene sulfonate) (PNaSS) is a strong polyelectrolyte, which has been proposed
43 for the control of biological and biophysical properties including enhancing cell adhesion,
44 spreading, and proliferation, thus improving bone tissue response[1,2], fibroblast behavior
45 for reconstructing injured ligament and wound healing[2–5], antibacterial infection[6] and
46 biocompatible surface[5,7]. PNaSS enhances the biological properties of PNaSS-grafted
47 surfaces: the mechanism at the origin of this activity involves specific interactions between
48 adsorbed binding proteins (fibronectin, FN) on functionalized surfaces and integrin at the
49 cell membrane[1,2]. Briefly, the presence of sulfonate groups allows improving cell
50 adhesion, proliferation, differentiation and/or biointegration in surrounding tissues when
51 implanted in vivo[1]. This has been shown in vitro with different types of cells (fibroblast,
52 endothelial cell, and osteoblast) and in vivo in the case of PNaSS-grafted titanium, PET and
53 PCL implants. PNaSS immobilized on different materials such as titanium[1,8], polyethylene
54 terephthalate (PET)[2,3], nanoparticle[5,9,10] or polycaprolactone (PCL) has been reported.

55 Several surface functionalization methods with poly(styrene sulfonate) have been proposed,
56 e.g. sulfonation polystyrene brush [10,11] and grafting methods[12–14]. Among those,
57 “grafting-from” has the advantage of being a scalable approach to the modification of
58 interfacial properties through immobilizing the functional groups on the substrate by
59 covalent bonding. The “grafting from” method starts with activation of the surface via
60 plasma[15], UV irradiation[7,16], heating[14,18], in the presence of CuBr₂[18–20], or Mohr's
61 salt[13,14].

62 In this work, we activate PET surfaces by ozonation, a method convenient for materials with
63 complex geometries such as implants[21]. Ozonation generates peroxide groups which
64 decompose upon heating and UV irradiation[14,22,27] to generate radicals on PET; NaSS
65 polymerizes from these active sites. The mechanism can be described as: the peroxides after
66 decomposition form two types of free radicals, $\cdot\text{OH}$ and $\text{O}\cdot$, and then $\text{C}\cdot$ (carbonyl)
67 radicals[21] on the polymer chains. Free radicals $\cdot\text{OH}$ can be consumed by Fe^{2+} in Mohr's
68 salt, thus reducing homopolymerization and promoting grafting[14,23,24].

69 Previous studies examined the effect of the graft PNaSS on the interaction of the modified
70 surfaces with biological molecules yet the characterization of the grafted layer is often
71 limited. Here, we investigate the topography of grafted polymers by atomic force
72 microscopy (AFM) complemented by XPS and contact angle measurements.

73

74 **2. Materials and Methods**

75 **2.1. Materials**

76 Sodium 4- styrene sulfonate (NaSS), phosphate buffer saline (PBS), and Mohr's salt were
77 purchased from Sigma Aldrich. Polyethylene terephthalate (PET) (0.25 mm, biaxially
78 oriented plate) was purchased from Goodfellow (Paris, France). Ethanol absolute was from
79 Fisher.

80 **2.1.1. PET preparation:**

81 PET plate was cut into small squared pieces (1 cm × 1 cm). The surface was cleaned in an
82 ultrasonic bath with ultrapure water, acetone, and ethanol for 10 min respectively. The
83 samples were dried under vacuum for 2 h and stored at 4°C until use.

84 **2.1.2. Monomer purification:**

85 The purification of NaSS was described [14,17,25] 90 g of NaSS was dissolved in 1.6 L of
86 ethanol: distilled water (9:1, v/v) by stirring 12 h at 70°C. Thereafter, the solution was
87 filtered by vacuum filtration. The filtered solution was kept at 4°C during 24 h for
88 recrystallization. Recrystallized monomer was collected by vacuum filtration and was dried
89 in vacuum at 30°C for 6 h. Finally, the product was kept at 4°C, away from the light.

90

91 **2.2. Functionalization of polyester surfaces by PNaSS (“grafting from”)**

92 **2.2.1. Activating the surfaces by ozonation**

93 The functionalization of polyesters by PNaSS includes two main steps: ozonation and
94 grafting (Scheme 1). In the first step, the polymer surfaces were activated by ozonation
95 using ozone generator BMT 802N. 6 PET plates were ozonized into 100 mL distilled water by
96 introducing ozone flow (0.6 bars, 100 mL/min) for 20 min for PET at 30° C.[14] Ozonized
97 samples were quickly transferred from the ozonation reactor to the degassed NaSS solution
98 (0.7 mol/L) for grafting.

99 **2.2.2. Grafting PNaSS from PET substrate**

100 After activation by ozonation, PNaSS was polymerized from the activated sites (Scheme 1).
101 For determining the influence of ozonation on the surface, non-grafted-ozonized polymer or
102 ozonized PET without grafting was used as a reference. Non-grafted-ozonized PET was
103 prepared by ozonation of a PET plate for 20 min at 30°C.

104 **Thermal radical polymerization (method 1 and 2):**

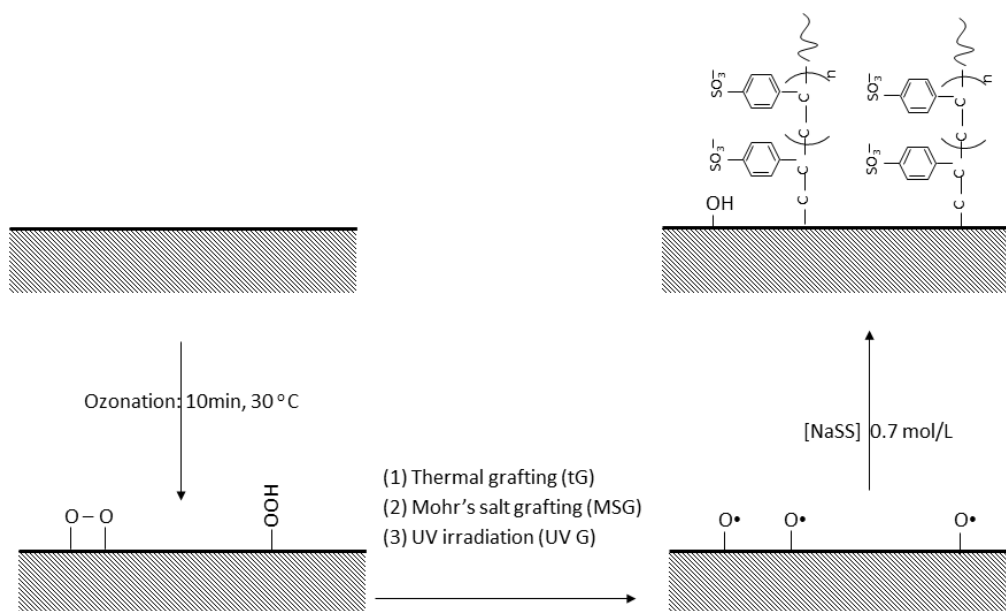
105 **Method 1 - Thermal grafting (TG)**[13,14]. 6 ozonized PET plates were transferred into 60 mL
106 of degassed NaSS (0.7 mol/L) solution and heated for 1 h at 75°C. Peroxide decomposition
107 generates the radicals on the surface for initiating PNaSS polymerization.

108 **Method 2-Thermal grafting in the presence of Mohr's salt (MSG).** 6 ozonized PET plates
109 were transferred into 60 mL degassed mixture solution of NaSS (9 g, 0.7 mol/L) and Mohr's
110 salt (60 mg, 0.1 %, w/v) and heated to 75°C for 1 h. Mohr's salt provides Fe(II) ions that
111 increases significantly the grafting efficiency[14].

112 **Photoinitiated free radical polymerization (method 3):**

113 **Method 3-UV irradiation (UVG)[22].** Peroxides were decomposed by UV irradiation. 6 PET
114 plates were transferred into 60 mL of degassed NaSS solution (9 g, 0.7 mol/L). The solution
115 was irradiated by UV light for 30 min (lamp UV-Omnigure, 254 nm, 10 W/cm²) at 25°C under
116 stirring.

117 After polymerization via either of the three methods above, free homopolymer, oligomer,
118 and monomer were removed from the grafted samples under stirring in double distilled
119 water for at least 48 h. The washing solution was tested by UV-vis at 360 nm to check for
120 the presence of any residue of free PNaSS (homopolymer and oligomer). Samples were
121 finally dried under vacuum and kept at 4°C, away from the light before use.



123 **Scheme 1. Grafting PNaSS from polyester surfaces by ozonation and radical polymerization**

124

125 **2.3. Surface characterization**

126 **X-ray photoelectron spectroscopy analysis (XPS).** X-ray photoelectron spectroscopy analysis
127 (XPS) (from Omicron Argus spectrometer, Germany) was performed using a
128 monochromated AlK α radiation source ($h\nu = 1486.6$ eV) working at an electron beam power
129 of 300 W with 90° of takeoff angle of photoelectrons emission, under ultra-high vacuum
130 ($\leq 10^{-10}$ Torr). Spectra were recorded at pass energy of 100 eV for the survey spectrum and
131 pass energy of 20 eV for the high-resolution regions. Binding energies were calibrated

132 against the C1s binding energy of aliphatic carbon atoms at 284.8 eV. Spectral
 133 deconvolution was carried out using Casa XPS v.2.3.15 software (Casa Software Ltd, UK). All
 134 samples were dry films.

135 The equivalent thickness probed by XPS is estimated to be close to $3\lambda = 10$ nm representing
 136 95% of the signal, λ being the inelastic mean free path of electrons from the PET substrate in
 137 the organic PNaSS film; for electrons having a kinetic energy around 1200 eV (from the C1s
 138 atomic level), λ is estimated to be equal to 3.23 nm.¹

139 The estimated thickness (d) of PNaSS on top of PET can then be calculated using the
 140 following formula:

$$\frac{I_{S2p}}{I_{C1s\ 284\ eV}} = \frac{\rho_{PNaSS} M_{ET} \sigma_{S2p} T_{S2p} \lambda_{S2p}^{PNaSS} \left(1 - \exp\left(\frac{-d}{\lambda_{S2p}^{PNaSS} \sin(\theta)}\right)\right)}{\rho_{PET} M_{NaSS} \sigma_{C1s} T_{C1s} \lambda_{C1s}^{PET} \left(\frac{-d}{\lambda_{C1s}^{PNaSS} \sin(\theta)}\right)}$$

141
 142 Wherein: θ is the photoelectron collection angle. TC1s and TS2p are the relative sensitivity
 143 factors of C and S, respectively, provided by the spectrometer manufacturer. The Scofield
 144 photoionization cross-sections σ are equal to 1 for C 1s and 1.44 for S2p.² $\lambda_x y$ is the inelastic
 145 mean free paths of electrons x in the matrix y . They were calculated using the Quases
 146 program (QUASES-IMFP-TPP2M Ver.3.0) based on the TPP2M formula. ρ_{PNaSS} and ρ_{PET} are
 147 the density of PNaSS and PET, respectively. M_{NaSS} and M_{ET} are the molecular weight of NaSS
 148 (sodium styrene sulfonate) and ET (ethylene terephthalate), respectively.

149

150 **Contact angle.** DSA10 contact angle system from KRUSS GmbH was used to measure the
 151 surface tension by the sessile drop technique. Two solvents: water (polar), and
 152 diiodomethane (unpolar) (2 μ L, 25°C, 8s) were used. The surface tension of polymer (γ_s) was
 153 calculated by Young-Dupre and Fowker's equation[26].

154 **Atomic Force Microscopy.** Atomic force microscope (AFM) multimode-8 from Bruker was
 155 used. AFM scans were carried out in air using Scanasyst probe (ScanAsyst cantilever (Silicon

¹ Tanuma, S.; Powell, C. J.; Penn, D. R. Calculation of electron inelastic mean free paths (IMFPs) VII. Reliability of the TPP-2M IMFP predictive equation. *Surf. Interface Anal.* 2003, 35, 268–275.

² Scofield J (1976) Hartree–Slater subshell photoionization cross-sections at 1254 and 1487 eV. *J Electron Spectrosc Relat Phenom* 8(2):129–37

156 Nitride), triangular, reflective aluminium, symmetric tip with radius ≤ 10 nm, f_0 : 70 KHz,
157 spring constant: ~ 0.4 N/m), scan rate 1 Hz, at different scan sizes: $500\text{ nm} \times 500\text{ nm}$, $2\text{ }\mu\text{m} \times$
158 $2\text{ }\mu\text{m}$ (3 samples). The absolute calibration was performed for each cantilever: Deflection
159 Sensitive, Spring Constant (~ 0.4 N/m) using Thermal Tuning and Lorentzian fitting (air), and
160 Tip Radius by Tip Qualification on Titanium roughness sample for PeakForce QNM (from
161 BRUKER). Samples were dried in vacuum chamber in 4 h before scanning. Scanning was
162 performed in the room conditions. 3 independent surfaces in the same grafting conditions
163 were analyzed. The roughness (Ra) was measured on 3 points/surface.

164 Nano-Scope Analysis v.1.5, Image-J and AtomicJ software[27] were used for image analysis.
165 Surface mechanical properties was measured by Peakforce Quantitative Nano-mechanical
166 Properties (PF-QNM) program[28]. When numbers of samples are indicated, they refer to
167 independent experiments (from sample preparation).

168

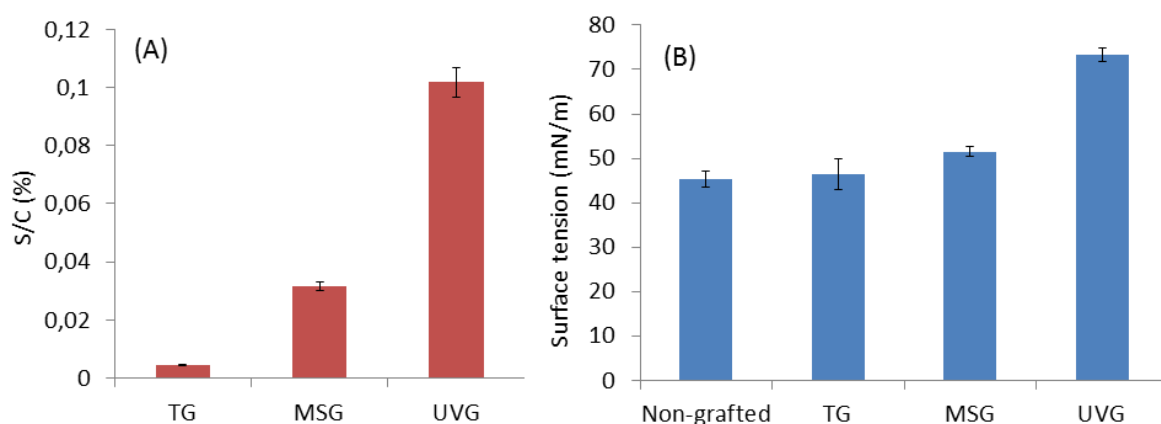
169 **3. Results**

170 **3.1. Surface characterization**

171 As a NaSS unit contains one atom of sulfur, the surface density of grafted PNaSS can be
172 estimated based on the percentage of sulfur atoms in the elementary composition using
173 XPS. Sulfur was not detected on the non-grafted-ozonized PET surfaces, but the S2p peak
174 was visible (165 – 170 eV)[29] on the 4 grafted surfaces (see high resolution spectra in
175 [Figure S1](#)). The quantification of those contributions indicated that the monomer surface
176 density was much lower in the case of the thermal grafting than for the UV and Mohr's salt
177 catalyzed grafting ([Figure 1A](#)).

178 Specifically, the S/C ratio for the UV and Mohr's salt samples was more than ten times
179 higher than for thermal grafting ([Figure 1A](#)). The PNaSS surface density (SD) by UV
180 irradiation was higher than when using Mohr's salt. The ranking was $SD_{\text{UVG-PET}} > SD_{\text{MSG-PET}} >$
181 $SD_{\text{TG-PET}}$. Whilst the XPS confirms the presence of PNaSS, the % S/C values themselves are
182 small indicating that the layers are thin and most probably patchy. Indeed, a rough estimate
183 value for the UVG PNaSS average layer thickness of 0.05 nm can be deduced from a simple
184 homogeneous model based on the depth probed by XPS being equal to 10 nm ([Figure S2](#))
185 and calculations thereafter.

186 Nevertheless, the surfaces were more hydrophilic after functionalization (Figure S3) and the
187 surface energy showed some correlation with the XPS results. The surface tension (γ_s) of
188 functionalized surfaces was measured by the contact angle method (Figure 1B). Non-grafted
189 and TG-PETs were similar: ~ 45 - 48 mN/m. However, surface tension increased significantly
190 on UV grafting samples. Particularly, γ_s of UVG-PET increased by 54 % (73 mN/m) and 8 %
191 for MSG-PET (~ 52 mN/m). These variations correlate with the amount of SO_3^- groups (%
192 Sulfur by XPS) on the surface leading to the increase of surface tension (represented by the
193 S/C ratio in Figure 1A).



194
195 Figure 1. Surface characterization of non-grafted-ozonized and grafted PET: (a) S/C ratio
196 from XPS and (b) surface tension by contact angle

198 3.2. Investigating structure of PNaSS-grafted PET surface by AFM

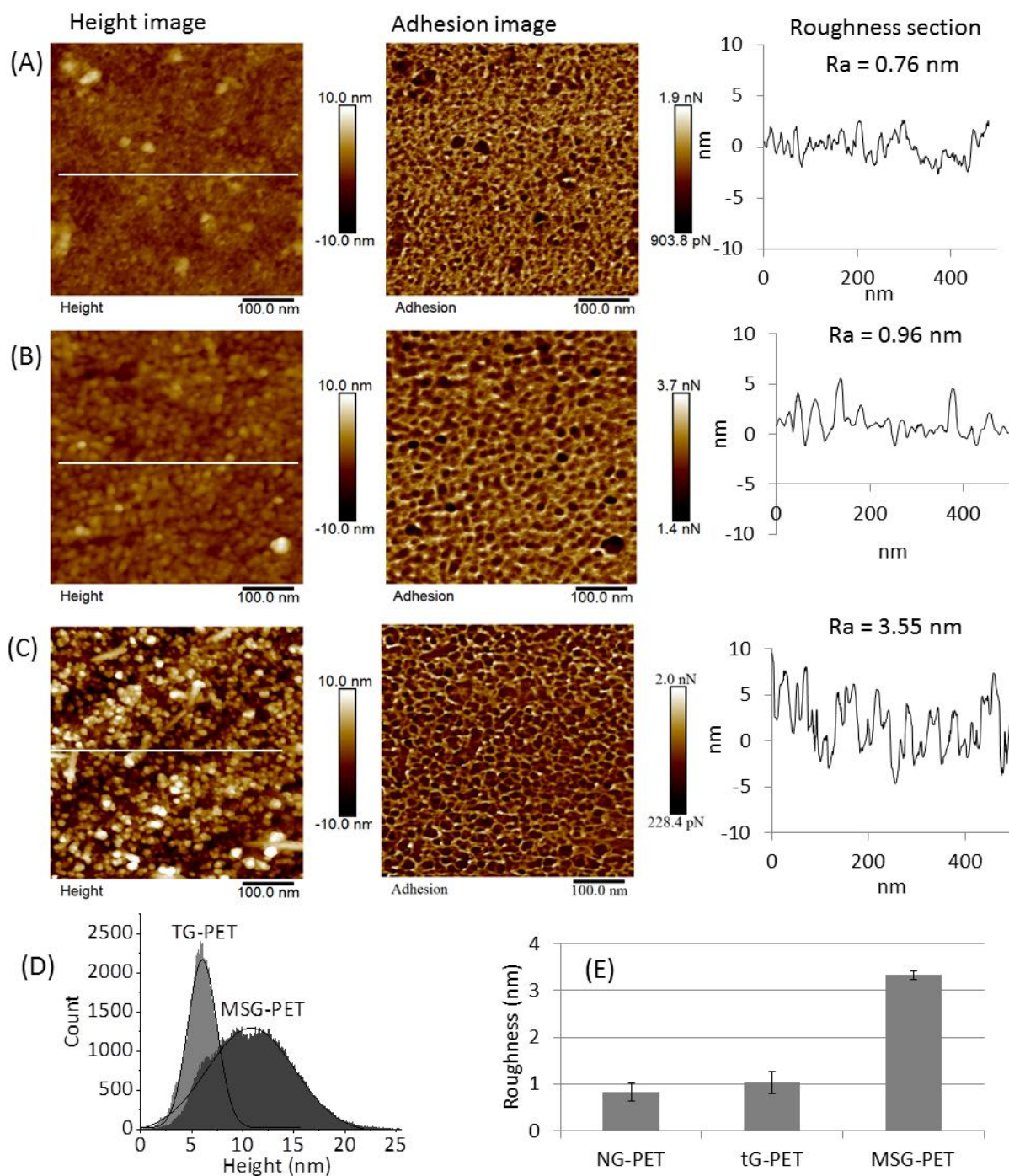
199 The surface SEM images showed no obvious changes (Figure S4). Therefore, in this work, we
200 investigated the grafted surface using atomic force microscope (AFM). AFM can be used as a
201 non-destructive method to analyze polymer surfaces[28,30–33]. Numerous parameters can
202 be investigated, e.g. the macromolecule structure[18], thickness[34–39], and adhesion.
203 PNaSS-grafted PET surfaces were investigated by AFM peak force Quantitative Nano-
204 mechanical properties (PF-QNM) in air at room temperature and compared to non-grafted-
205 ozonized surface. Adhesion maps measure the interaction between the AFM tip and the
206 material : they can therefore provide clues as to the local chemical nature of the
207 surface[40].

208 The surface topography and adhesion images of non-grafted-ozonized PET were used as a
209 reference. The AFM images of the PET surfaces obtained after PNaSS grafting by the thermal
210 grafting and Mohr's salt grafting methods are shown in [Figure 2](#) and briefly described below.

211 **Thermal radical polymerization:**

212 **Thermal grafting.** TG-PET surface topography and adhesion were similar to the non-grafted-
213 ozonized surface ([Figure 2A-B](#)). This was in agreement with the XPS and contact angle
214 results which suggested a low degree of grafting. The surface roughness of TG-PET ($R_a =$
215 0.76 nm)-was similar with that of non-grafted PET ($R_a = 0.96$ nm), see in [Figure 2E](#).

216 **Thermal grafting in the presence of Mohr's salt.** The topography of MSG-PET appeared
217 similar but the surface roughness ($R_a = 3.55$ nm, see in [Figure 2C](#)) increased by a factor 3
218 ([Figure 2E](#)).



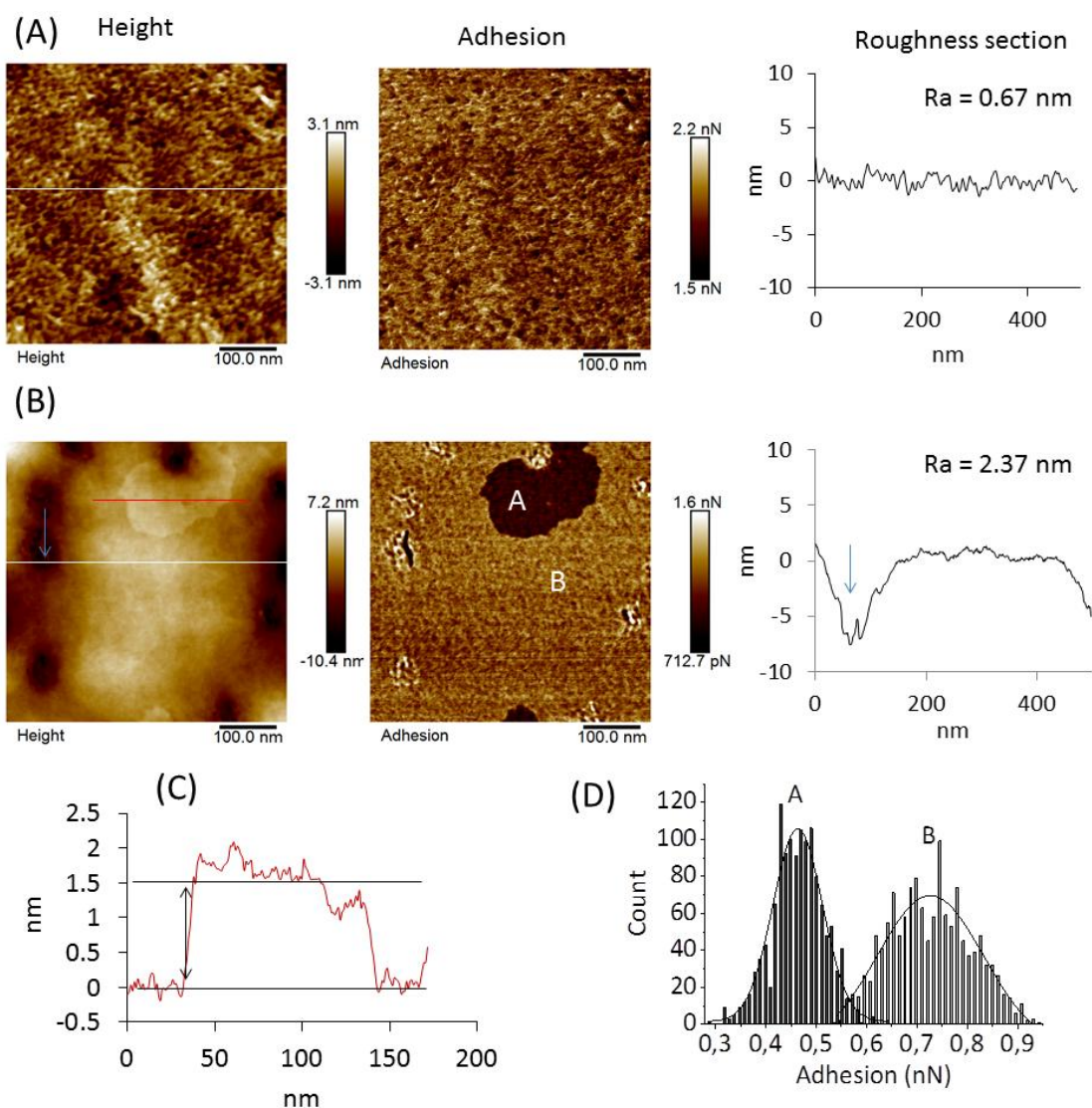
219

220 Figure 2. AFM images of non-grafted and thermal grafted PET: (A) non-grafted-ozonized PET
 221 without grafting, (B) thermal grafting (TG-PET), (C) thermal grafting in the presence of
 222 Mohr's salt (MSG-PET), (D) Height distribution of TG-PET and MSG-PET, (E) Roughness
 223 values for each method; Scan in air, scan size 500 nm x 500 nm, 256 points/line, scan rate 1
 224 Hz, PF-QNM

225

226 **Photoinitiated radical polymerization:**

227 **UV grafting (UVG).** Remarkably, in the case of UV grafting, both topography and adhesion
228 images (Figure 3) were drastically different from what had been observed in the other cases.
229 To evaluate whether the UV treatment itself had an effect on surface topography, a control
230 sample was prepared with non-grafted-ozonized PET under UV irradiation for 30 min
231 without monomer. No major difference between this UV control (Figure 3A) and the non-
232 grafted-ozonized control (Figure 2A) were observed. To the contrary, a smoother surface
233 was observed on UV grafted PET with patches particularly striking in the adhesion image
234 (Figure 3B). The patch shown in Figure 3C is ~ 1.5 nm thick (red line) and with reduced
235 adhesion (Figure 3D). An average thickness of the patches can be deduced from multiple
236 measurements of different patches (~ 1.2 nm, $n = 5$, Figure S5). Taking into account the
237 surface covered by the patches ($\sim 8\%$ of the total area, Figure S5) the thickness averaged
238 overall the whole area is ~ 0.09 nm ($8\% \times 1.2$ nm), consistent with the XPS results (~ 0.05 nm,
239 see above and Figure S2) suggesting that those patches are indeed composed of PNaSS.



240

241 Figure 3. AFM images of UV grafted PET (A) Control sample (ozonized PET under UV
 242 irradiation without monomer), (B) UV grafted PET, (C) Particular Cross-section by red line,
 243 and (D) Adhesion force distribution (flat surface, patches); scan size 500 nm x 500 nm, 256
 244 points/line, scan rate 1 Hz, PF-QNM

245

246 4. Discussion

247 The combination of the XPS, surface tension and AFM images suggest the following picture
 248 of the grafted surfaces. The thermal grafting results indicate a low grafting (XPS results,
 249 Figure 1A) on PET. This correlates with the surface tension measurements where we do not
 250 observe significant changes from the unmodified surfaces (Figure 1B). The AFM images of
 251 those surfaces in dry air may not allow visualization of the PNaSS in the case of thermal

252 grafting. The absence of detectable change in the case of thermal grafting is probably due to
253 a combination of low grafting (as indicated by XPS and surface tension) and of the fact that
254 the non-grafted-ozonized PET surface is already rough making it harder to detect small
255 changes.

256 In the case of thermal grafting in the presence of Mohr's salt, XPS and surface tension
257 measurements correlate and both point to an increased functionalization. The AFM images
258 show an increased roughness (Figure 2 and Figure S6) but this increase cannot be attributed
259 to PNaSS because we know from the XPS results that on average the PNaSS layer is only of
260 the order of ~ 0.02 nm suggesting a low coverage of thin patches (Figure S2). Instead, the
261 increase of the surface roughness is probably caused by surface degradation in the presence
262 of Mohr's salt redox initiator as previously reported [40].

263 In the case of photoinitiated radical polymerization (UV grafting), again XPS and surface
264 tension measurements correlate (Figure 1). Compared to Mohr's salt, they point to an
265 increased PNaSS surface density for PET. In the AFM images we observe ~ 1 nm thick patches
266 covering 8% of the surface and with markedly reduced adhesion. We interpret those
267 patches as being PNaSS patches since they correspond to the average thickness estimated
268 by XPS. We note that the rest of the surface show a different (smoother) structure
269 compared to the control. We used an ozonized PET under UV irradiation in distilled water to
270 evaluate if changes to surface topology could have been caused by the UV irradiation
271 treatment but that does not seem to be the case. Further investigations will be needed to
272 determine what causes the smoothing of the PET surface during PNaSS grafting by UV
273 irradiation. Another limitation of our interpretation of the results is that those unexplained
274 topography changes could have contributed to the variations of contact angle
275 independently of PNaSS coverage.

276

277 5. Conclusion

278 PNaSS was successfully immobilized by ozonation activation and thermal grafting or UV
279 grafting. The results provide insights into the morphology of PNaSS grafted on polyethylene
280 terephthalate that is commonly used in biomedical engineering by harnessing a
281 combination of AFM-Peakforce Quantitative Nanomechanical properties with XPS and
282 contact angle measurements. Average thicknesses in the nm or sub-nm range determined

283 by XPS indicate a low PNaSS coverage. In the case of UV grafting 1 nm thick discrete patches
284 covering ~ 8% of the surface were observed. Some surface reconstruction happening during
285 PNaSS grafting will need to be explored in further work. As said in the introduction, the
286 reported findings would allow precisising how the pNaSS molecules can interact with specific
287 proteins as fibronectin and by this with cells. A lot of in vitro and in vivo biological results
288 were obtained and published on pNaSS grafted PET and this precise and fine view in the
289 structure of the grafted molecules will be a perfect tool to perfect the elucidation of the
290 mechanism of the biological activity of such surfaces.

291

292 **Funding Sources**

293 This work was funded as part of the "Future Investment Project" by the French Public
294 Investment Bank (BPI) and the French state - PSPC application - Liga2bio project.

295

296 **References**

- 297 [1] Felgueiras H P, Sommerfeld S D, Murthy N S, Kohn J and Migonney V 2014 Poly(NaSS)
298 functionalization modulates the conformation of fibronectin and collagen type i to
299 enhance osteoblastic cell attachment onto Ti6Al4V *Langmuir* **30** 9477–83
- 300 [2] Vaquette C, Viateau V, Guérard S, Anagnostou F, Manassero M, Castner D G and
301 Migonney V 2013 The effect of polystyrene sodium sulfonate grafting on
302 polyethylene terephthalate artificial ligaments on invitro mineralisation and invivo
303 bone tissue integration *Biomaterials* **34** 7048–63
- 304 [3] Curti P S, Moura M R D, Veiga W, Radovanovic E, Rubira A F and Muniz E C 2005
305 Characterization of PNIPAAm photografted on PET and PS surfaces *Appl. Surf. Sci.* **245**
306 223–33
- 307 [4] Elbert D L, Herbert C B and Hubbell J A 1999 Thin polymer layers formed by
308 polyelectrolyte multilayer techniques on biological surfaces *Langmuir* **15** 5355–62
- 309 [5] Girard J, Brunetto P S, Braissant O, Rajacic Z, Khanna N, Landmann R, Daniels A U and
310 Fromm K M 2013 Development of a polystyrene sulfonate/silver nanocomposite with

- 311 self-healing properties for biomaterial applications *Comptes Rendus Chim.* **16** 550–6
- 312 [6] Simoes J A, Citron D M, Aroutcheva A, Anderson R A, Chany C J, Waller D P, Faro S
313 and Zaneveld L J D 2002 Two novel vaginal microbicides (polystyrene sulfonate and
314 cellulose sulfate) inhibit *Gardnerella vaginalis* and anaerobes commonly associated
315 with bacterial vaginosis *Antimicrob. Agents Chemother.* **46** 2692–5
- 316 [7] Chouirfa H, Evans M D M, Bean P, Saleh-Mghir A, Crémieux A C, Castner D G,
317 Falentin-Daudré C and Migonney V 2018 Grafting of Bioactive Polymers with Various
318 Architectures: A Versatile Tool for Preparing Antibacterial Infection and
319 Biocompatible Surfaces *ACS Appl. Mater. Interfaces* **10** 1480–91
- 320 [8] Chouirfa H, Evans M D M, Castner D G, Bean P, Mercier D, Galtayries A, Falentin-
321 Daudré C and Migonney V 2017 Grafting of architecture controlled poly(styrene
322 sodium sulfonate) onto titanium surfaces using bio-adhesive molecules: Surface
323 characterization and biological properties *Biointerphases* **12** 02C418
- 324 [9] Harris C M, Miller S G, Andresen K and Thompson L B 2018 Quantitative
325 measurement of sodium polystyrene sulfonate adsorption onto CTAB capped gold
326 nanoparticles reveals hard and soft coronas *J. Colloid Interface Sci.* **510** 39–44
- 327 [10] Su N, Li H B, Zheng H M, Yi S P and Liu X H 2012 Synthesis and characterization of
328 poly(sodium-p-styrenesulfonate)/modified SiO₂ spherical brushes *Express Polym.*
329 *Lett.* **6** 680–6
- 330 [11] Moujahid E M, Besse J P and Leroux F 2002 Synthesis and characterization of a
331 polystyrene sulfonate layered double hydroxide nanocomposite. In-situ
332 polymerization vs. polymer incorporation *J. Mater. Chem.* **12** 3324–30
- 333 [12] Börner H G, Duran D, Matyjaszewski K, Da Silva M and Sheiko S S 2002 Synthesis of
334 molecular brushes with gradient in grafting density by atom transfer polymerization
335 *Macromolecules* **35** 3387–94
- 336 [13] Rohman G, Huot S, Vilas-Boas M, Radu-Bostan G, Castner D G and Migonney V 2015
337 The grafting of a thin layer of poly(sodium styrene sulfonate) onto poly(ϵ -
338 caprolactone) surface can enhance fibroblast behavior *J. Mater. Sci. Mater. Med.* **26**
339 206

- 340 [14] Nguyen T N, Rangel A A, Migonney V, Nguyen N T, Rangel A A and Migonney V 2020
341 Kinetic and degradation reactions of poly (sodium 4-styrene sulfonate) grafting
342 “from” ozonized poly (ϵ -caprolactone) surfaces *Polym. Degrad. Stab.* **176** 109154
- 343 [15] Lego B, Skene W G and Giasson J S 2008 Unprecedented covalently attached ATRP
344 initiator onto OH-functionalized mica surfaces *Langmuir* **24** 379–82
- 345 [16] Mathis C H, Simič R, Kang C, Ramakrishna S N, Isa L and Spencer N D 2019 Indenting
346 polymer brushes of varying grafting density in a viscous fluid: A gradient approach to
347 understanding fluid confinement *Polymer (Guildf)*. **169** 115–23
- 348 [17] Ciobanu M, Siove A, Gueguen V, Gamble L J, Castner D G and Migonney V 2006
349 Radical graft polymerization of styrene sulfonate on poly(ethylene terephthalate) films
350 for ACL applications: “Grafting from” and chemical characterization
351 *Biomacromolecules* **7** 755–60
- 352 [18] Yamamoto S, Ejaz M, Tsujii Y and Fukuda T 2000 Surface interaction forces of well-
353 defined, high-density polymer brushes studied by atomic force microscopy. 2. Effect
354 of graft density *Macromolecules* **33** 5608–12
- 355 [19] Yamamoto S, Tsujii Y and Fukuda T 2000 Atomic force microscopic study of stretching
356 a single polymer chain in a polymer brush *Macromolecules* **33** 5995–8
- 357 [20] Jones D M, Brown A A, Huck W T S, Street P and Cb C 2002 Surface-Initiated
358 Polymerizations in Aqueous Media: Effect of Initiator Density Darren *Langmuir* 1265–
359 9
- 360 [21] Fujimoto K, Takebayashi Y, Inoue H and Ikada Y 1993 Ozone-induced graft
361 polymerization onto polymer surface *J. Polym. Sci. Part A Polym. Chem.* **31** 1035–43
- 362 [22] Amokrane G, Falentin-Daudré C, Ramtani S and Migonney V 2018 A Simple Method
363 to Functionalize PCL Surface by Grafting Bioactive Polymers Using UV Irradiation *Irbm*
364 **39** 268–78
- 365 [23] Ishigaki I, Sugo T, Takayama T, Okada T, Okamoto J and Machi S 1982 Graft
366 polymerization of acrylic acid onto polyethylene film by preirradiation method. II.
367 Effects of oxygen at irradiation, storage time after irradiation, mohr’s salt, and

- 368 ethylene dichloride *J. Appl. Polym. Sci.* **27** 1043–51
- 369 [24] Fujimoto K, Tadokoro H, Ueda Y and Ikada Y 1993 Polyurethane surface modification
370 by graft polymerization of acrylamide for reduced protein adsorption and platelet
371 adhesion *Biomaterials* **14** 442–8
- 372 [25] Pavon-Djavid G, Gamble L J, Ciobanu M, Gueguen V, Castner D G and Migonney V
373 2007 Bioactive poly(ethylene terephthalate) fibers and fabrics: Grafting, chemical
374 characterization, and biological assessment *Biomacromolecules* **8** 3317–25
- 375 [26] Frederick M. Fowkes and Fowkes F M 1964 Attractive Forces At Interfaces *Ind. Eng.*
376 *Chem.* **56** 40–52
- 377 [27] Hermanowicz P, Sarna M, Burda K and Gabryś H 2014 AtomicJ: An open source
378 software for analysis of force curves *Rev. Sci. Instrum.* **85**
- 379 [28] Pittenger B, Erina N, Su C, Mapping M P, Pittenger B, Erina N and Su C 2010
380 Quantitative Mechanical Property Mapping at the Nanoscale with PeakForce QNM
381 *Bruker Appl. Note AN128 AN128* 12
- 382 [29] Goh S H, Lee S Y, Zhou X and Tan K L 1999 X-ray Photoelectron Spectroscopic Studies
383 of Interactions between Styrenic Polymers and Poly(2,6-dimethyl-1,4-phenylene
384 oxide) *Macromolecules* **32** 942–4
- 385 [30] Nair S S, Wang C and Wynne K J 2019 AFM Peakforce QNM mode for measurement
386 of nanosurface mechanical properties of Pt-cured silicones *Prog. Org. Coatings* **126**
387 119–28
- 388 [31] Young T J, Monclus M A, Burnett T L, Broughton W R, Ogin S L and Smith P A 2011
389 The use of the PeakForce™ quantitative nanomechanical mapping AFM-based
390 method for high-resolution Young's modulus measurement of polymers *Meas. Sci.*
391 *Technol.* **22**
- 392 [32] Dokukin M E and Sokolov I 2012 Quantitative mapping of the elastic modulus of soft
393 materials with HarmoniX and PeakForce QNM AFM modes *Langmuir* **28** 16060–71
- 394 [33] Kaemmar S B 2011 Introduction to Bruker's ScanAsyst and PeakForce Tapping AFM
395 Technology *Appl. note* **133** 12

- 396 [34] Sui X, Zapotoczny S, Benetti E M, Schön P and Vancso G J 2010 Characterization and
397 molecular engineering of surface-grafted polymer brushes across the length scales by
398 atomic force microscopy *J. Mater. Chem.* **20** 4981–93
- 399 [35] Chen W L, Cordero R, Tran H and Ober C K 2017 50th Anniversary Perspective:
400 Polymer Brushes: Novel Surfaces for Future Materials *Macromolecules* **50** 4089–113
- 401 [36] Halperin A and Zhulina E B 2010 Atomic force microscopy of polymer brushes:
402 Colloidal versus sharp tips *Langmuir* **26** 8933–40
- 403 [37] Phillips R W 1994 Atomic force microscopy for thin film analysis *Surf. Coatings*
404 *Technol.* **68–69** 770–5
- 405 [38] Lego B, Skene W G and Giasson S 2010 Swelling study of responsive polyelectrolyte
406 brushes grafted from mica substrates: Effect of pH, salt, and grafting density
407 *Macromolecules* **43** 4384–93
- 408 [39] Variola F 2015 Atomic force microscopy in biomaterials surface science *Phys. Chem.*
409 *Chem. Phys.* **17** 2950–9
- 410 [40] Zalakain I, Politakos N, Ramos J A, Saralegi A, Etxeberria H, Mondragon I, Corcuera M
411 A and Eceiza A 2013 Chemical and morphological characterization of sulfonated
412 polystyrene brushes in different environments *Eur. Polym. J.* **49** 2120–7

413

414 **Declaration of interests**

415 The authors declare that they have no known competing financial interests or personal
416 relationships that could have appeared to influence the work reported in this paper.

417

418 **Author Contributions**

419 **Tuan Ngoc Nguyen:** [principal technical contributor, conception, design and conduct of the](#)
420 [experiments, acquisition, analysis, interpretation of data, initial draft the work.](#) **Raphaël**
421 **Lévy:** [Interpretation of data, draft and substantively revised the work.](#) **Vincent Humblot:**
422 [acquisition, analysis, interpretation of data.](#) **Véronique Migonney:** [supervisor, project](#)
423 [conception, draft and substantively revised the work.](#)

424 All authors have approved the submitted version

425